Video Article

Liquid-cell Transmission Electron Microscopy for Tracking Self-assembly of Nanoparticles

Byung Hyo Kim[1,2], Junyoung Heo[1,2], Won Chul Lee[3], Jungwon Park[1,2]

[1]Center for Nanoparticle Research, Institute for Basic Science (IBS)

[2]School of Chemical and Biological Engineering, Institute of Chemical Processes, Seoul National University

[3]Department of Mechanical Engineering, Hanyang University

Correspondence to: Won Chul Lee at wonchullee@hanyang.ac.kr, Jungwon Park at jungwonpark@snu.ac.kr

URL: https://www.jove.com/video/56335
DOI: doi:10.3791/56335

Keywords: Chemistry, Issue 128, Nanoparticles, self-assembly, solvent-drying, transmission electron microscopy, liquid cell TEM, *in situ* TEM

Date Published: 10/16/2017

Citation: Kim, B.H., Heo, J., Lee, W.C., Park, J. Liquid-cell Transmission Electron Microscopy for Tracking Self-assembly of Nanoparticles. *J. Vis. Exp.* (128), e56335, doi:10.3791/56335 (2017).

Abstract

Drying a nanoparticle dispersion is a versatile way to create self-assembled structures of nanoparticles, but the mechanism of this process is not fully understood. We have traced the trajectories of individual nanoparticles using liquid-cell transmission electron microscopy (TEM) to investigate the mechanism of the assembly process. Herein, we present the protocols used for liquid-cell TEM studies of the self-assembly mechanism. First, we introduce the detailed synthetic protocols used to produce uniformly sized platinum and lead selenide nanoparticles. Next, we present the microfabrication processes used to produce liquid cells with silicon nitride or silicon windows and then describe the loading and imaging procedures of the liquid-cell TEM technique. Several notes are included to provide helpful tips for the entire process, including how to manage the fragile cell windows. The individual motions of nanoparticles tracked by liquid-cell TEM revealed that changes in the solvent boundaries caused by evaporation affected the self-assembly process of nanoparticles. The solvent boundaries drove nanoparticles to primarily form amorphous aggregates, followed by flattening of the aggregates to produce a 2-dimensional (2D) self-assembled structure. These behaviors are also observed for different nanoparticle types and different liquid-cell compositions.

Video Link

The video component of this article can be found at https://www.jove.com/video/56335/

Introduction

The self-assembly of colloidal nanoparticles is of interest because it provides an opportunity to access collective physical properties of individual nanoparticles[11]. One of the most effective methods of self-assembly used in practical device-scale applications is self-organization of nanoparticles on a substrate through evaporation of a volatile solvent[6,7,8,9,10,11]. This solvent evaporation method is a nonequilibrium process, which is largely influenced by kinetic factors such as evaporation rate and changes in nanoparticle-substrate interactions. However, since it is difficult to estimate and control the kinetic factors, the mechanistic understanding of nanoparticle self-assembly by solvent evaporation is not fully mature. Although *in situ* X-ray scattering studies have provided ensemble-averaged information of the nonequilibrium nanoparticle self-assembly process[12,13,14], this technique cannot determine the motion of individual nanoparticles, and their association with the overall trajectory cannot be easily accessed.

Liquid-cell TEM is an emerging tool for tracking the trajectory of individual nanoparticles, enabling us to understand the inhomogeneity of nanoparticle motions and their contribution to ensemble behaviors[15,16,17,18,19,20,21,22,23,24,25,26]. We have previously used liquid-cell TEM to track the motion of individual nanoparticles during solvent evaporation, showing that the movement of the solvent boundary is a major driving force for inducing nanoparticle self-assembly on a substrate[18,19]. Herein, we introduce experiments where we can observe the process of nanoparticle self-assembly using liquid-cell TEM. First, we provide protocols for the synthesis of platinum and lead selenide nanoparticles, before introducing the fabrication procedures of liquid-cells for TEM and how to load nanoparticles into the liquid-cell. As representative results, we show snapshot images from TEM movies of nanoparticle self-assembly driven by solvent drying. By tracking individual particles in these movies, we can understand the detailed mechanisms of solvent-drying-mediated self-assembly at a single nanoparticle level. During self-assembly, the platinum nanoparticles on the silicon nitride window mainly follow the movement of the evaporating solvent front because of the strong capillary forces acting on the thin solvent layer. Similar phenomena were also observed for other nanoparticles (lead selenide) and substrates (silicon), indicating that the capillary force of the solvent front is an important factor in particle migration near a substrate.

Protocol

1. Synthesis of Nanoparticles

1. **Synthesis of platinum nanoparticles**
    1. Combine 17.75 mg of ammonium hexachloroplatinate(IV) ($(NH_4)_2Pt(IV)Cl_6$), 3.72 mg of ammonium tetrachloroplatinate(II) ($(NH_4)_2Pt(II)Cl_4$), 115.5 mg of tetramethylammonium bromide, 109 mg of poly(vinylpyrrolidone) (MW: 29,000), and 10 mL of ethylene glycol with a stir bar in a 100 mL 3-neck round bottom flask equipped with a rubber septum.
    2. Equip the flask with a reflux condenser and purge under vacuum. Stir the reaction mixture with a magnetic stir bar at 1,000 rpm.
    3. Heat the reaction mixture to 180 °C in a heating mantle at a rate of 10 °C/min under a flow of argon.
    4. Maintain the temperature (180 °C) for 20 min. The solution becomes a dark brown color.
    5. Remove the flask from the heating mantle to allow it to cool to room temperature.
    6. Transfer the product to a 50 mL centrifuge tube. Add 30 mL of acetone to the product to precipitate the nanoparticles and centrifuge the sample at 2,400 x g for 10 min.
       NOTE: For safety, this process should be performed in a fume hood.
    7. Discard the supernatant and re-disperse the black precipitate with 10 mL of ethanol.
    8. Precipitate the product with 30 mL of toluene and centrifuge the suspension at 2,400 x g for 10 min. Discard the supernatant and re-disperse the black precipitate with 10 mL of ethanol. Repeat this process 3 times.
    9. Add 5 mL of oleylamine to the platinum nanoparticles and transfer the dispersion to a 100 mL round-bottom flask. Reflux the dispersion overnight under magnetic stirring at 1,000 rpm to allow the ligand exchange reaction to occur.
    10. Centrifuge the ligand-exchanged nanoparticles at 10,000 x g for 30 min to separate them from the solution.
    11. Discard the supernatant and disperse the platinum nanoparticles in 10 mL of a hydrophobic solvent, such as toluene, hexane, or chloroform.

2. **Synthesis of lead selenide nanoparticles**
    1. Preparation of lead oleate
        1. Combine 758 mg of lead acetate trihydrate ($Pb(Ac)_2 \cdot 3H_2O$), 2.5 mL of oleic acid, and 10 mL of diphenyl ether with a stir bar in a 100 mL 3-neck round bottom flask equipped with a rubber septum.
        2. Equip the flask with a reflux condenser.
        3. Degas the mixture at 70 °C under vacuum condition for 2 h and stir with a magnetic stir bar at 1,000 rpm.
        4. Purge the flask with argon and then cool it to room temperature.

    2. Preparation of trioctylphosphine selenide (TOPSe)
        1. In a separate vessel, combine 474 mg of selenium and 6 mL of trioctylphosphine (TOP) under an inert atmosphere, using a glovebox to prevent exposure of the reagents to air.
        2. Dissolve selenium powder in TOP by ultrasonication at 110 W, 40 kHz, and mix using a vortex mixer until the solution becomes visibly transparent.

    3. In a separate 250 mL 3-neck round bottom flask, degas 15 mL of diphenyl ether at 120 °C under vacuum condition with magnetic stirring at 1,000 rpm for 30 min.
    4. Purge the flask with argon, and then heat the diphenyl ether to 230 °C.
    5. Rapidly inject both the lead oleate and the TOPSe solutions into the pre-heated diphenyl ether. The temperature will drop to some extent upon injection. Set the aging temperature to 170 °C.
    6. Maintain the temperature of the mixture at 170 °C for 10 min with vigorous stirring to allow the growth of lead selenide nanoparticles to occur.
    7. Remove the flask from the heating mantle to allow it to cool to room temperature.
    8. Prepare two 50 mL centrifuge tubes and divide the product into equal volumes and transfer to the tubes. Add 30 mL of ethanol to each tube to precipitate the nanoparticles and centrifuge the suspension at 2,400 x g for 10 min.
    9. Discard the supernatant and re-disperse the black precipitate with 10 mL of toluene.
    10. Precipitate the product with 30 mL of ethanol and centrifuge the suspension at 2,400 x g for 10 min. Discard the supernatant and re-disperse the black precipitate with 10 mL of toluene. Repeat this process 3 times.
    11. Discard the supernatant and disperse the lead selenide nanoparticles in 10 mL of a hydrophobic solvent, such as toluene, hexane, or chloroform.

2. Liquid-cell Fabrication

1. **Silicon nitride liquid-cell (Figure 3a)**
    1. Deposition of silicon nitride layer
        1. Deposit a low-stress silicon nitride film onto 100 µm-thick silicon wafers (4 inch) by low-pressure chemical vapor deposition (LPCVD) at 835 °C and a pressure of 140 mTorr with a flow of 100 sccm dichlorosilane and 50 sccm ammonia. Control the thickness of silicon nitride layer to be ~25 nm by varying the deposition time. The deposition rate is 2.5 - 3.0 nm/min, but varies slightly for each CVD.

    2. Top and bottom chips
       NOTE: Please refer to reference[25] for a detailed description of the microfabrication process.

1. Spin coat 10 mL of positive photoresist on the silicon nitride/silicon wafer at 3,000 rpm for 30 s, using enough photoresist to wet the wafer completely.
   NOTE: Ultrathin silicon wafers are easily broken during spinning. We usually attach the ultrathin wafer on another silicon wafer with a thickness of 500 µm using photoresist to avoid breakage. After spin-coating, the thin wafer is separated from the thick wafer by immersion in acetone. This technique can also be used in the following process for spin coating on ultrathin silicon wafers.
2. Bake the wafer on a hot plate at 85 °C for 60 s.
   NOTE: Do not bake the prepared wafer at temperatures of >110 °C. Baking the photoresist at high temperatures will cause the photoresist to change from a positive to a negative photoresist.
3. Expose the photoresist-coated wafer to ultraviolet light (365 nm) for 10 s through a chromium mask (**Figure 1a**).
4. Immerse the photoresist-coated wafer into 50 mL of developer solution for 40 s. Soak the developed wafer in 50 mL of deionized water for 1 min to wash the wafer. Repeat the washing process twice.
5. Etch the silicon nitride for 1 min using a reactive ion etcher with a flow of 50 sccm of sulfur hexafluoride.
6. Immerse the top chip and bottom chip in acetone for 2 min to remove the photoresist. Shake the dish gently by hand to effectively remove the photoresist.
7. Etch the silicon with an aqueous solution of potassium hydroxide (30 mg/mL) at 85 °C for 1.5 - 2 h. Use a water bath to ensure that the etching solution has a uniform temperature profile. Uneven temperature will lead to some areas being excessively etched while some are incompletely etched.
8. When the window appears to be completely etched by the naked eye, stop the etching and take the cell out of the etching solution. Tilt the cell when removing it from the etching solution to avoid the chance of the window being broken by buoyancy, which can occur if lifted horizontally.
9. Repeat these procedures with a mask for the bottom chip (**Figure 1b**).
   NOTE: As the windows of the top and bottom chip are very thin, about 25 nm, they are very fragile. Therefore, extreme care should be taken when handling. The window side should always be facing upwards when the chip is rested on a surface.

3. Bonding top and bottom chips
   1. Spin coat 10 mL of positive photoresist on the silicon nitride/silicon wafer at 3,000 rpm for 30 s.
   2. Bake the wafer on a hot plate at 90 °C for 60 s.
   3. Expose the photoresist-coated wafer to ultraviolet light (365 nm) for 10 s through a chromium mask (**Figure 1c**).
   4. Immerse the photoresist-coated wafer into 50 mL of developer solution for 40 s. Soak the developed wafer in 50 mL of deionized water for 1 min to wash the wafer. Repeat the washing process twice.
   5. Deposit a ~100 nm thick layer of indium onto the bottom chip using a thermal evaporator. The indium layer is used as both a spacer and a sealing material.
   6. Immerse the chip in acetone for 2 min to remove the photoresist. Shake the dish gently by hand to effectively remove the photoresist.
   7. Align the bottom and top chips using an aligner and bond them at 100 °C.

2. **Silicon liquid-cell (Figure 3b)**
   1. Preparation of top and bottom chips
      1. Use p-type silicon-on-insulator (SOI) wafers with layer thicknesses of 100 nm, 400 nm, and 600 µm for the top silicon, buried SiO_2, and handling silicon layers, respectively.
      2. Perform wet oxidation of the SOI wafer in an oxidation furnace at 950 - 1100 °C to grow a layer of silicon oxide with a thickness of 170 nm.
      3. Etch the silicon oxide by dipping the SOI wafer into a buffered oxide etch (BOE) solution at room temperature for 2 min, which is a wet etchant of silicon oxide. The purpose of steps 2.2.1.2 and 2.2.1.3 is to reduce the thickness of the top silicon layer of the SOI wafer to 25 nm.
      4. Deposit a layer of low-stress silicon nitride with a thickness of 25 nm onto the SOI wafers (4-inch) by LPCVD using the same process conditions as in step 2.1.1.1.
      5. Pattern the silicon nitride using the same processes and mask patterns as in steps 2.1.2.1 - 2.1.2.4.
      6. Immerse the wafers in acetone for 2 min to remove the photoresist. Shake the dish gently by hand to effectively remove the photoresist.
      7. Etch the silicon oxide with the BOE solution for 30 s.
      8. Etch the silicon with an aqueous solution of potassium hydroxide (500 mg/mL) at 80 °C for 7 - 12 h. Trimethylamine hydroxide (TMAH) aqueous solution can also be used for the silicon etching.
      9. Etch the silicon nitride with 85 % phosphoric acid at 160 °C for 10 min.
      10. Etch the silicon oxide with the BOE solution at room temperature for 3 min.
      11. Repeat the procedures of steps 2.2.1.1 - 2.2.1.10 with a mask for the bottom chip (**Figure 1b**).

   2. Bonding top and bottom chips
      1. Spin coat 10 mL of positive photoresist on the silicon nitride/silicon wafer at 3,000 rpm for 30 s.
      2. Bake the wafer on a hot plate at 90 °C for 60 s.
      3. Expose the photoresist-coated wafer to ultraviolet light (365 nm) for 10 s through a chromium mask (**Figure 1c**).
      4. Immerse the photoresist-coated wafer into 50 mL of developer solution for 40 s. Soak the developed wafer in 50 mL of deionized water for 1 min to wash the wafer. Repeat the washing process twice.
      5. Deposit a ~100 nm thick layer of indium onto the bottom chip using a thermal evaporator. The indium layer is used as both a spacer and a sealing material.
      6. Immerse the chip in acetone for 2 min to remove the photoresist. Shake the dish gently by hand to effectively remove the photoresist.

7. Align the bottom and top chips using an aligner and bond them at 100 °C.

3. Liquid-cell TEM

1. **Loading solution**
   1. Add 20 µL of the nanoparticle dispersion (protocol 1.1 and 1.2) into a 5 mL vial and dry in the air for 10 min. Disperse the nanoparticles in a solvent mixture (1 mL of o-dichlorobenzene, 250 µL of pentadecane, and 10 µL of oleylamine).
   NOTE: Drying under extreme conditions, such as high temperature, low pressure, and for extended durations may result in poor nanoparticle dispersions. Since the ligand-to-particle interactions are dynamic, there is a high probability of the agglomeration of particles after ligand detachment under extreme conditions. Since o-dichlorobenzene, pentadecane, and oleylamine have different vapor pressures, the drying process should be carried out immediately before the loading process to keep the solvent ratio constant.
   2. Inspect the liquid-cell using an optical microscope.
   NOTE: If any of the windows of a liquid-cell are broken, do not use the cell.
   3. Load ~100 nL of the nanoparticle dispersion into the reservoirs (**Figure 2a** and **2b**) of the liquid-cell. An injector equipped with an ultrathin capillary (**Figure 2c**) can be used to load the small amount of dispersion into reservoirs of the liquid-cell effectively.
   NOTE: In general, the injected amount of nanoparticle dispersion exceeds the capacity of the reservoir. If the dispersion overflows from the reservoir, the liquid-cell may not completely seal. Therefore, any overflowing dispersion outside the reservoir must be absorbed by the tip of a filter paper cut into a fan shape. Avoid contact with the window during absorption.
   4. Expose the liquid-cell to the air for 10 min to dry the o-dichlorobenzene.
   5. Apply vacuum grease to one side of a copper aperture grid with a size of 2 mm and a hole-size of 600 µm and cover the liquid-cell with the greased side of the aperture grid to create a sealed environment.
   NOTE: Vacuum grease deposited on the window greatly reduces the TEM resolution. Thus, failure to match the hole of the copper aperture grid with the window of the cell on the first attempt should not be corrected; rather, the cell should be discarded and a new one prepared.

2. **TEM measurement**
   1. Place the liquid-cell in a standard TEM holder. The liquid-cell is designed to fit into a standard holder.
   NOTE: Use gloves to avoid contamination of the TEM holder.
   2. Set the TEM in continuous image acquisition mode. Capture TEM images at an acceleration voltage of 200 kV with a current density of ~700 A/m^2.
   NOTE: Frequently check the TEM pressure level. If the pressure level is abnormal, stop imaging immediately and remove the holder from the TEM chamber as quickly as possible. The low contrast of the liquid-cell TEM causes difficulty in focusing the image. Fine alignment and focusing can be performed easily by an initial coarse focus on edge of the window. The drying rate can be controlled by changing the current density. The 2D drying rate can be measured by tracking the size of the evolving drying patches. However, it is difficult to quantify the drying rate in terms of volume.
   3. Open the original TEM images using the ImageJ software package. Select the multi-point icon of the program and assign the centers of all the individual nanoparticles of the image, and then extract the x and y coordinates of the selected particles.
   4. Calculate the radial distribution function (RDF):

$$g(r) = \frac{1}{2\pi r\rho}\frac{1}{N}\sum_{j=1}^{N}\sum_{k\neq j}^{N}\delta\left(r - \left|r_{jk}\right|\right) = \frac{A}{\pi r N^2}\sum_{j=1}^{N-1}\sum_{k=j+1}^{N}\delta\left(r - \left|r_{jk}\right|\right)$$

   where r is the interparticle distance, N is the number of particles, A is the area covered by the particles, ρ is 2D areal density of particles (N/A), r_{jk} is the position vector from particle j to particle k, and $\delta(r)$ is the Dirac delta function. We use $\frac{1}{a\sqrt{\pi}}\exp\left(-r^2/a^2\right)$, where a = 0.8 nm as the Dirac delta function for the realistic calculation.

Representative Results

The liquid-cell is composed of a top chip and a bottom chip, which are equipped with silicon nitride windows that are transparent to an electron beam with a thickness of 25 nm. The top chip has a reservoir for storing the sample solution and evaporated solvent. The chips are made via conventional microfabrication processing[25]. The masks used for the top and bottom chips are shown in **Figure 1a** and **1b**, respectively. **Figure 2a** and **2b** show images of the top and bottom chips, respectively. The chips are separated by a 100 nm-thick spacer to allow the nanoparticle solution to be loaded (**Figure 1c**). We also fabricated silicon liquid-cells from SOI wafers. Through the patterning and etching process, liquid-cells having silicon windows with a thickness of 25 nm are obtained. The fabrication processes for silicon nitride and silicon liquid-cells are shown in **Figure 3**.

The self-assembly of platinum nanoparticles in a silicon nitride liquid-cell was studied using the liquid-cell TEM. **Figure 4** shows the temporal motion of nanoparticles during solvent evaporation. As the solvent evaporates from various points, the solvent front moves and the nanoparticles are dragged by the solvent front. This interface-mediated motion occurs because of the strong capillary forces of the thin solvent layer and reduced free energy when the particles are at the interface.

A similar interface-mediated motion of nanoparticles was also observed for lead selenide nanoparticles (**Figure 5**). Nanoparticles move along the solvent front. Assembled domains grow by the addition of nanoparticles that are dragged by the capillary forces of the thin solvent layer. In addition, platinum nanoparticles on silicon substrates exhibit similar behavior to those on silicon nitride substrates (**Figure 6**).

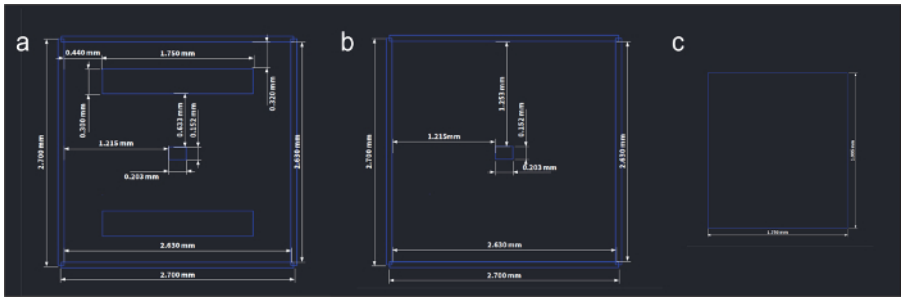

Figure 1: Brief illustration of the three masks used for patterning the (**a**) top chips, (**b**) bottom chips, and (**c**) spacers. Please click here to view a larger version of this figure.

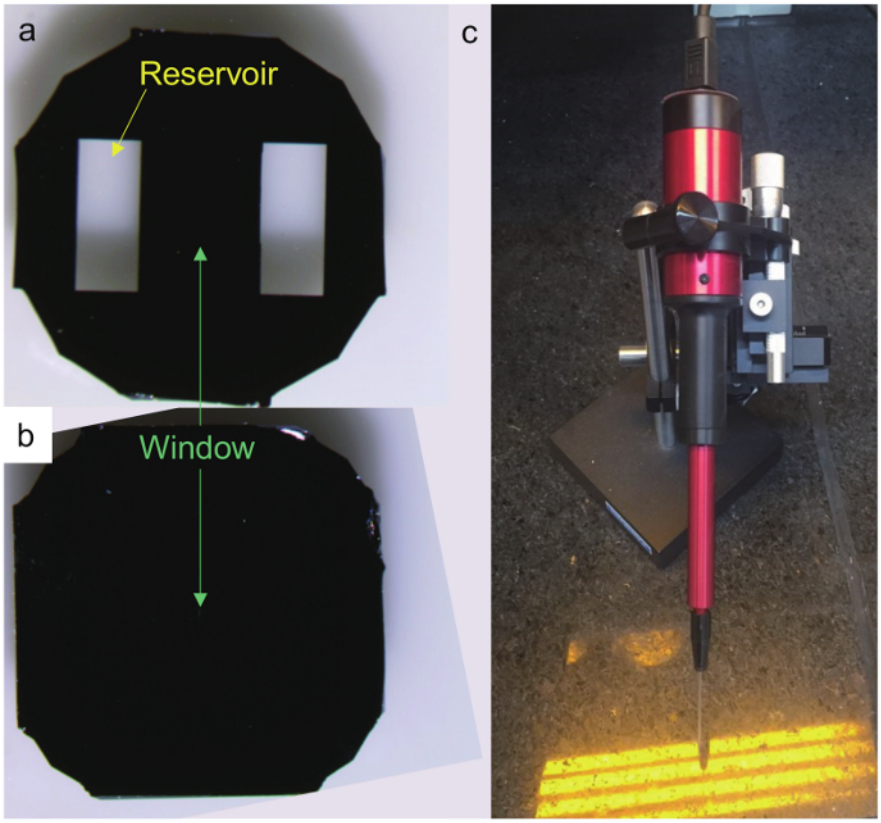

Figure 2: Optical microscopy image of (**a**) a top chip and (**b**) a bottom chip. (**c**) Image of the loading instrument equipped with an ultrathin capillary. Please click here to view a larger version of this figure.

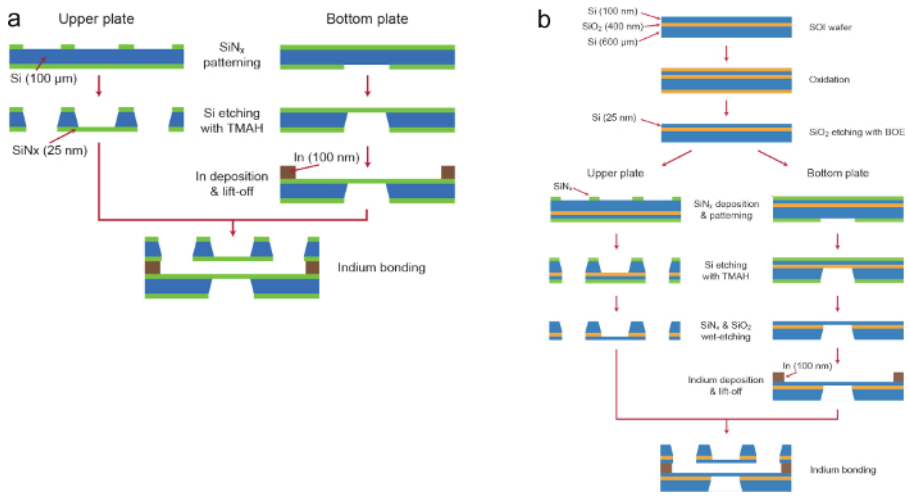

Figure 3: Schematic diagram of fabrication processes of (**a**) the silicon nitride liquid-cell and (**b**) the silicon liquid-cell. Reprinted with permission from American Chemical Society[19]. Please click here to view a larger version of this figure.

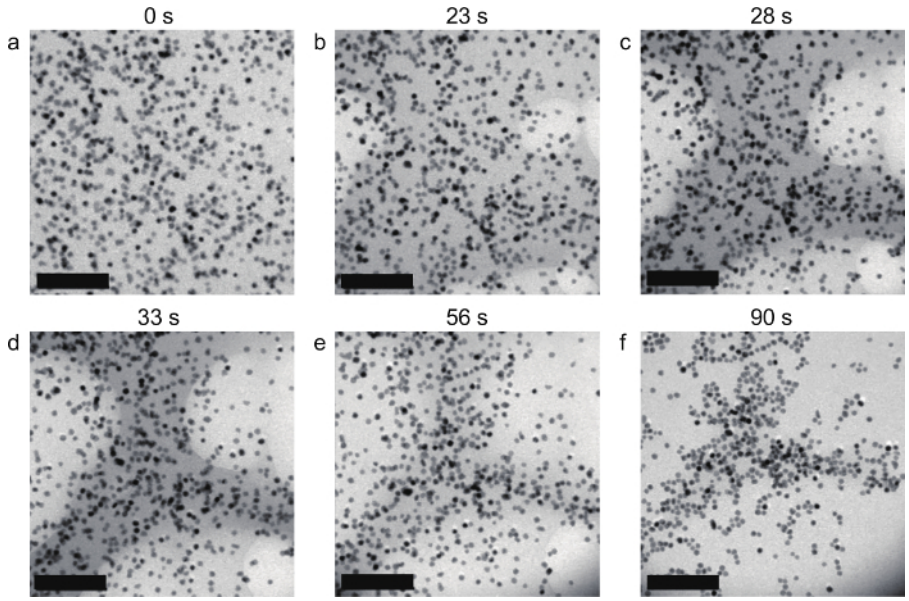

Figure 4: Snapshot images of the liquid-cell from a movie recorded by TEM of the solvent-drying-mediated self-assembly of platinum nanoparticles in a silicon nitride liquid-cell. The images were taken at (**a**) 0 s, (**b**) 23 s, (**c**) 28 s, (**d**) 33 s, (**e**) 56 s, and (**f**) 90 s. Scale bars = 100 nm. Please click here to view a larger version of this figure.

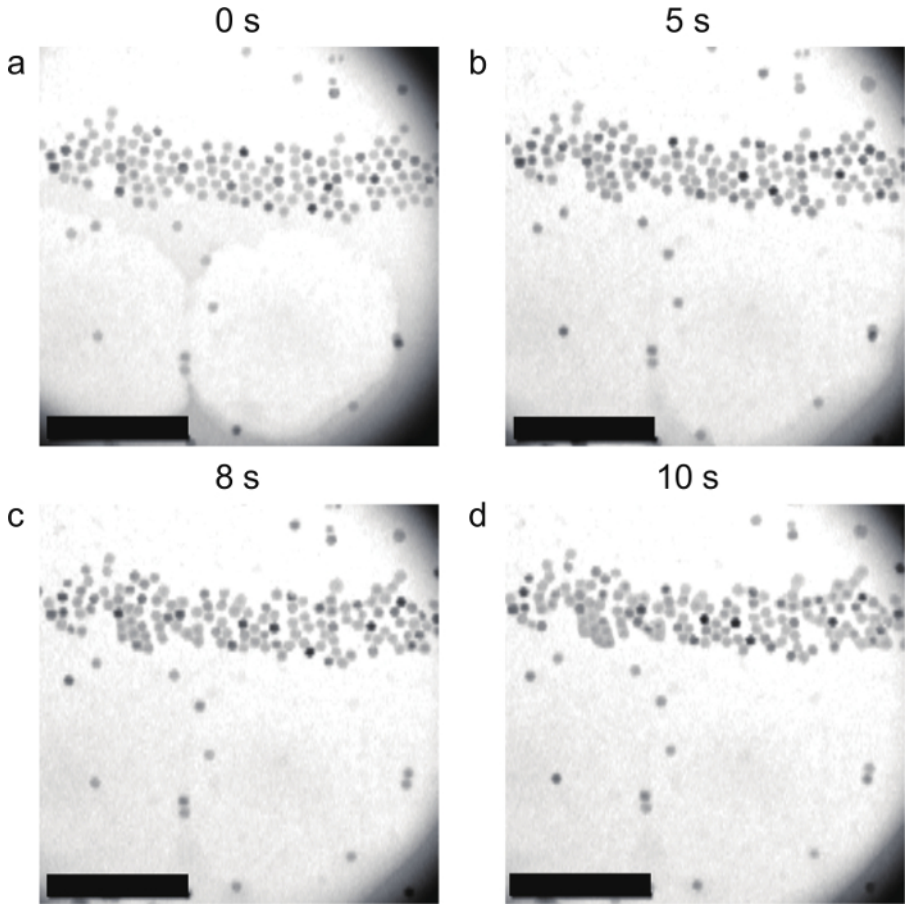

Figure 5: Snapshot images of the liquid-cell from a movie recorded by TEM of the solvent-drying-mediated self-assembly of lead selenide nanoparticles in a silicon nitride liquid-cell. The images were taken at (**a**) 0 s, (**b**) 5 s, (**c**) 8 s, and (**d**) 10 s. Scale bars = 200 nm. Please click here to view a larger version of this figure.

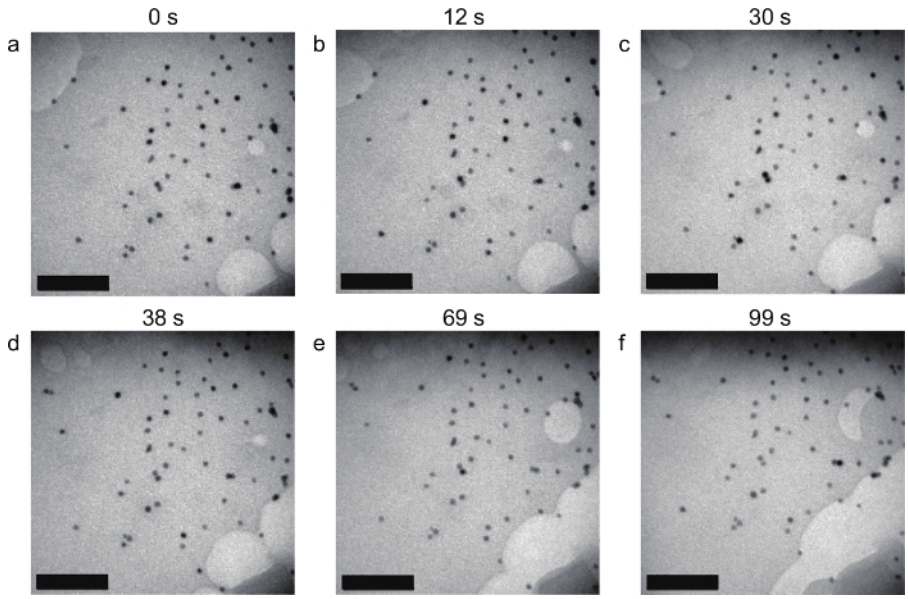

Figure 6: Snapshot images of the liquid-cell from a movie recorded by TEM of the solvent-drying-mediated self-assembly of platinum nanoparticles in a silicon liquid-cell. The images were taken at (**a**) 0 s, (**b**) 12 ,s (**c**) 30 s, (**d**) 38 s, (**e**) 69 s, and (**f**) 99 s. Scale bars = 100 nm. Please click here to view a larger version of this figure.

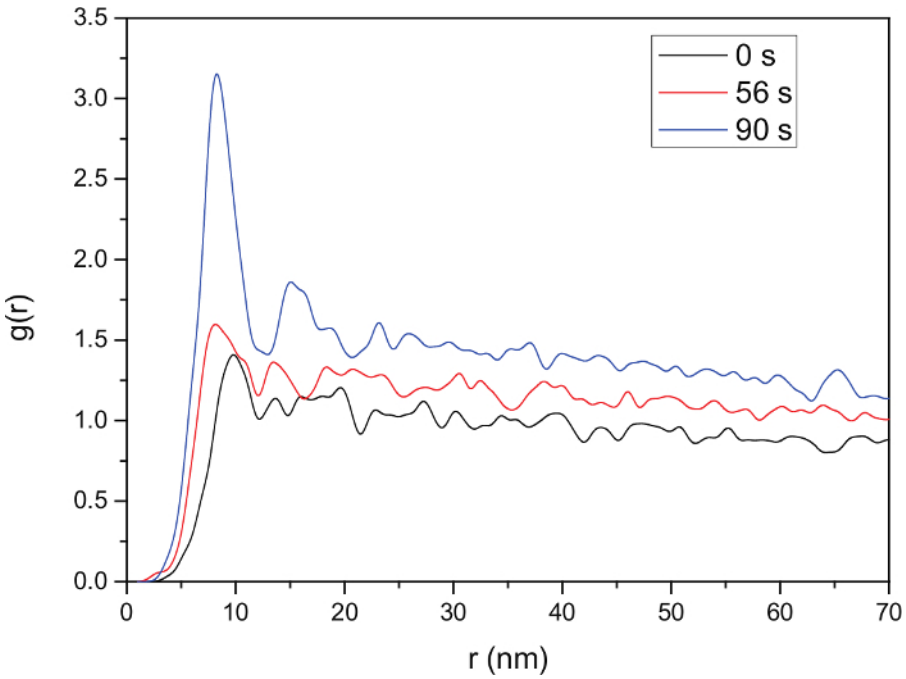

Figure 7: Radial distribution function (RDF) of platinum nanoparticles in a silicon nitride liquid-cells at (black) 0 s, (red) 56 s, and (blue) 90 s in Figure 4. Please click here to view a larger version of this figure.

Discussion

Platinum nanoparticles with a size of 7 nm were synthesized via the reduction of ammonium hexachloroplatinate (IV) and ammonium tetrachloroplatinate (II) using poly (vinylpyrrolidone) (PVP) as a ligand and ethylene glycol as a solvent and a reducing agent[27]. A ligand-exchange reaction with oleylamine was performed to disperse the particles in a hydrophobic solvent. Lead selenide nanoparticles were synthesized via the thermal decomposition of lead-oleate complexes using TOP-Se as a selenium source[28] (Refer to reference[29] for the detailed synthesis of chalcogenide nanocrystals). Since the as-synthesized lead selenide nanoparticles were already capped with long-chain ligands, the particles did not require a ligand-exchange process. Hydrophobic platinum and lead selenide nanoparticles were dispersed in a mixed solvent composed of o-dichlorobenzene, pentadecane, and oleylamine. O-dichlorobenzene, which has a relatively low boiling point (180.5 °C), presumably evaporates during solution loading, but pentadecane, which has a high boiling point (270 °C), remains after o-dichlorobenzene evaporation. A trace amount of oleylamine was added as an additional surfactant to prevent aggregation of the nanoparticles.

We fabricated liquid-cells that were compatible with conventional TEM holders using routine microfabrication techniques to obtain TEM images of nanoparticles in solution[25]. The masks used to fabricate the top and bottom chips are shown in **Figure 1**. The silicon nitride windows of the cell are very thin (25 nm) so careful handling during the process is required. There are a few situations that are likely to cause the fragile windows to break. Firstly, placing the liquid-cells window-side down on surfaces may cause the windows to break because of friction. Also, when the cells are taken out of the etching solution, the buoyancy of the solution may break the windows. In addition, the windows may break during the drying of the washing solution with an air flow, so the air should be blown horizontally with a weak intensity.

The platinum and lead selenide nanoparticle dispersions in the mixed solvent are loaded into a large rectangular-shaped reservoir of the liquid-cells. The solution flows into the center of the cells where the windows are located, because of capillary forces. Using an injector equipped with ultrathin capillary helps to load a small amount of dispersion into the cells effectively. The cells are sealed by covering them with copper aperture grids, to which vacuum grease has been applied. Care should also be taken not to break the cell windows during the assembly of the cells. If breakage of a cell window is found, the liquid-cell should never be inserted into a TEM chamber.

We observed nanoparticle motion in real-time using the liquid-cell TEM technique. The TEM images have relatively dark and bright areas because of the varying thickness of the solution (**Figure 4**). The dark areas, corresponding to relatively thick areas of the solution, shrunk continuously under irradiation by the electron beam. This change can be induced by solvent drying, bubble formation, or dewetting.[30] Among them, the change in contrast shown in **Figure 4** seems to be caused by solvent drying, rather than bubble formation or dewetting. When bubble formation occurs, bright areas of circular or elliptical shapes appear and dynamically merge, but this phenomenon is not seen in **Figure 4**[31]. On the other hand, considering the hydrophobic silicon nitride surface and hydrophobicity of the solvent used, the dewetting effect is insignificant.

Figure 4 shows the self-assembly process of the platinum nanoparticles as the solvent of the particle dispersion evaporates. The solvent-drying-mediated self-assembly of nanoparticles is composed of several steps. First, the nanoparticles condense into amorphous agglomerates with several layers by the rapidly moving solvent. Secondly, these agglomerates flatten onto the substrate to form a monolayer. Finally, local solvent fluctuations result in an ordered structure of nanoparticles. We tracked particle positions at three different times (0 s, 56 s, and 90 s) and quantitatively analyzed the assembly by calculating the RDF at these times (**Figure 7**). At t = 0 s, the RDF shows only a small peak near 10 nm, indicating the particles are randomly distributed. As the solvent evaporates, nanoparticles move closer together, and the RDF peak shifts to a

shorter distance. The RDF shows a strong peak near 8.3 nm at 90 s. Considering the size of the nanoparticles (7.3 nm) and the length of the ligands (~1 nm), the RDFs indicate that the particles are assembled at the closest distance possible upon solvent drying.

The initial stage of the self-assembly process of lead selenide nanoparticles is similar to that of platinum particles (**Figure 4** and **Figure 5**). In the next stage, however, the assembly process of lead selenide nanoparticles differs from that of platinum. **Figure 5b** shows that the nanoparticles were self-assembled with a gap between the nanoparticles, indicating the existence of surfactants on the nanoparticle surfaces. After 8 seconds, however, these gaps disappear, and the nanoparticles are attached together. Finally, the nanoparticles melt and aggregate. The TEM images show that surface atoms of the lead selenide nanoparticles diffused quickly. Through the liquid-cell TEM analysis, we can analyze the reason why lead selenide nanoparticles form a unique self-assembled structure that forms a direct bond between particles.

We have demonstrated the multi-step mechanism of nanoparticle self-assembly driven by solvent evaporation using liquid-cell TEM. Liquid-cell TEM enables the observation of not only the self-assembly process but also the growth process, attachment, and transformation of nanoparticles. The experimental tools will help to understand nanoparticle motion that is not revealed by conventional *in situ* techniques.

Disclosures

The authors have nothing to disclose.

Acknowledgements

We thank Prof. A. Paul Alivisatos at the University of California, Berkeley and Prof. Taeghwan Hyeon at Seoul National University for the helpful discussion. This work was supported by IBS-R006-D1. W.C.L. gratefully acknowledges support from the research fund of Hanyang University (HY-2015-N).

References

1. Shevchenko, E. V., Talapin, D. V., Kotov, N. A., O'Brien, S., Murray, C. B. Structural Diversity in Binary Nanoparticle Superlattices. *Nature.* **439,** 55-59 (2006).
2. Talapin, D. V., et al. Quasicrystalline Order in Self-Assembled Binary Nanoparticle Superlattices. *Nature.* **461,** 964-967 (2009).
3. Evers, W. H., Friedrich, H., Filion, L., Dijkstra, M., Vanmaekelbergh, D. Observation of a Ternary Nanocrystal Superlattice and Its Structural Characterization by Electron Tomography. *Angew. Chem., Int. Ed.* **48,** 9655-9657 (2009).
4. Maillard, M., Motte, L., Pileni, M. P. Rings and Hexagons Made of Nanocrystals. *Adv. Mater.* **13**, 200-204 (2001).
5. Sztrum, C. G., Rabani, E. Out-of-Equilibrium Self-Assembly of Binary Mixtures of Nanoparticles. *Adv. Mater.* **18,** 565-571 (2006).
6. Han, W., Lin, Z. Learning From "coffee Rings": Ordered Structures Enabled by Controlled Evaporative Self-Assembly. *Angew. Chem., Int. Ed.* **51,** 1534-1546 (2012).
7. Bigioni, T. P., et al. Kinetically Driven Self Assembly of Highly Ordered Nanoparticle Monolayers. *Nat. Mater.* **5,** 265-270 (2006).
8. Govor, L. V., Reiter, G., Parisi, J., Bauer, G. H. Self-Assembled Nanoparticle Deposits Formed at the Contact Line of Evaporating Micrometer-Size Droplets. *Phys. Rev. E.* **69,** 61609 (2004).
9. Kletenik-Edelman, O., et al. Drying-Mediated Hierarchical Self-Assembly of Nanoparticles: A Dynamical Coarse-Grained Approach. *J. Phys. Chem. C.* **112,** 4498-4506 (2008).
10. Kletenik-Edelman, O., Sztrum-Vartash, C. G., Rabani, E. Coarse-Grained Lattice Models for Drying-Mediated Self-Assembly of Nanoparticles. *J. Mater. Chem.* **19,** 2872-2876 (2009).
11. Rabani, E., Reichman, D. R., Geissler, P. L., Brus, L. E. Drying-Mediated Self-Assembly of Nanoparticles. *Nature.* **426,** 271-274 (2003).
12. Loubat, A., et al. Growth and Self-Assembly of Ultrathin Au Nanowires into Expanded Hexagonal Superlattice Studied by in Situ SAXS. *Langmuir.* **30,** 4005-4012 (2014).
13. Connolly, S., Fullam, S., Korgel, B., Fitzmaurice, D. Time-Resolved Small-Angle X-Ray Scattering Studies of Nanocrystal Superlattice Self-Assembly. *J. Am. Chem. Soc.* **120,** 2969-2970 (1998).
14. Lu, C., Akey, A. J., Dahlman, C. J., Zhang, D., Herman, I. P. Resolving the Growth of 3D Colloidal Nanoparticle Superlattices by Real-Time Small-Angle X-Ray Scattering. *J. Am. Chem. Soc.* **134,** 18732-18738 (2012).
15. Zheng, H., Claridge, S. A., Minor, A. M., Alivisatos, A. P., Dahmen, U. Nanocrystal Diffusion in a Liquid Thin Film Observed by in Situ Transmission Electron Microscopy. *Nano Lett.* **9,** 2460-2465 (2009).
16. Jungjohann, K. L., Bliznakov, S., Sutter, P. W., Stach, E. A., Sutter, E. A. In Situ Liquid Cell Electron Microscopy of the Solution Growth of Au-Pd Core-Shell Nanostructures. *Nano Lett.* **13,** 2964-2970 (2013).
17. Yuk, J. M., et al. High-Resolution EM of Colloidal Nanocrystal Growth Using Graphene Liquid Cells. *Science.* **336,** 61-64 (2012).
18. Park, J., et al. Direct Observation of Nanoparticle Superlattice Formation by Using Liquid Cell Transmission Electron Microscopy. *ACS Nano.* **6,** 2078-2085 (2012).
19. Lee, W. C., Kim, B. H., Choi, S., Takeuchi, S., Park, J. Liquid Cell Electron Microscopy of Nanoparticle Self-Assembly Driven by Solvent Drying. *J. Phys. Chem. Lett.* **8,** 647-654 (2017).
20. Park, J., et al. 3D Structure of Individual Nanocrystals in Solution by Electron Microscopy. *Science.* **349,** 290-295 (2015).
21. Chee, S. W., Baraissov, Z., Loh, N. D., Matsudaira, P. T., Mirsaidov, U. Desorption-Mediated Motion of Nanoparticles at the Liquid-Solid Interface. *J. Phys. Chem. C.* **120,** 20462-20470 (2016).
22. Liu, Y., Lin, X.-M., Sun, Y., Rajh, T. In Situ Visualization of Self-Assembly of Charged Gold Nanoparticles. *J. Am. Chem. Soc.* **135,** 3764-3767 (2013).
23. Verch, A., Pfaff, M., de Jonge, N. Exceptionally Slow Movement of Gold Nanoparticles at a Solid/Liquid Interface Investigated by Scanning Transmission Electron Microscopy. *Langmuir.* **31,** 6956-6964 (2015).
24. Sutter, E., et al. In Situ Microscopy of the Self-Assembly of Branched Nanocrystals in Solution. *Nat. Commun.* **7,** 11213 (2016).

25. Niu, K.-Y., Liao, H.-G., Zheng, H. Revealing Dynamic Processes of Materials in Liquid Using Transmission Electron Microscopy. *J. Vis. Exp.* **70,** e50122 (2012).
26. Hermannsdörfer, J., de Jonge, N. Studying Dynamic Processes of Nano-sized Objects in Liquid using Scanning Transmission Electron Microscopy. *J. Vis. Exp.* **120,** e54943 (2017).
27. Tsung, C. K., et al. Sub-10 nm Platinum Nanocrystals with Size and Shape Control: Catalytic Study for Ethylene and Pyrrole Hydrogenation. *J. Am. Chem. Soc.* **131,** 5816-5822 (2009).
28. Cho, K. S., Talapin, D. V., Gaschler, W., Murray, C. B. Designing PbSe Nanowires and Nanorings through Oriented Attachment of Nanoparticles. *J. Am. Chem. Soc.* **127,** 7140-7147 (2005).
29. Manthiram, K., Beberwyck, B. J., Talapin, D. V., Alivisatos, A. P. Seeded Synthesis of CdSe/CdS Rod and Tetrapod Nanocrystals, *J. Vis. Exp.* **82,** e50731 (2013).
30. Woehl, T. J., et al. Experimental Procedures to Mitigate Electron Beam Induced Artifacts During in situ Fluid Imaging of Nanomaterials. *Ultramicroscopy.* **127,** 53-63 (2013).
31. Shin, D., et al. Growth Dynamics and Gas Transport Mechanism of Nanobubbles in Graphene Liquid Cells. *Nat. Commun.* **6,** 6068 (2015).

